AGU100 ADVANCING EARTH AND SPACE SCIENCE

JGR

Journal of Geophysical Research: Biogeosciences

RESEARCH ARTICLE
10.1002/2017JG004165

Key Points:
- Anthropogenic nutrient enrichment alters the dynamics of microbial community on suspended sediment
- Microorganisms play an important role in modulating N cycle in suspended sediment
- Depolymerization of necromass contributes a control over the dynamics of N cycle

Supporting Information:
- Supporting Information S1
- Data Set S1
- Data Set S2
- Data Set S3

Correspondence to:
F. H. M. Tang,
fiona.tang@sydney.edu.au

Citation:
Tang, F. H. M., & Maggi, F. (2018). Biomodulation of nitrogen cycle in suspended sediment. *Journal of Geophysical Research: Biogeosciences*, *123*, 1230–1246. https://doi.org/10.1002/2017JG004165

Received 15 SEP 2017
Accepted 25 FEB 2018
Accepted article online 1 MAR 2018
Published online 13 APR 2018

Biomodulation of Nitrogen Cycle in Suspended Sediment

Fiona H. M. Tang[1] **and Federico Maggi**[1]

[1] Laboratory for Advanced Environmental Engineering Research, School of Civil Engineering, The University of Sydney, Sydney, New South Wales, Australia

Abstract Biogeochemical experiments and modeling were coupled to investigate how nutrient leaching to aquatic ecosystems changes the dynamics of microbial community on suspended sediment and how these changes modulate the nitrogen cycle. Mineral suspensions amended with inorganic nitrogen (NH_4^+ and NO_3^-) and inoculated with native sedimentary microbial strains were tested in a settling column under continuous water quality measurements. Experiments were used to calibrate and validate a kinetic model that explicitly described the chemical adsorption on minerals, aqueous complexation, gas dissolution, microbial metabolism, necromass dynamics, and microbial competition for limiting substrates. Modeling revealed that the interactions between microbial functional groups were highly nonlinear and highly sensitive to changes in nutrient and dissolved oxygen concentrations, showing shifts in regimes where a functional group became prevalent over the others. Our results suggested that necromass dynamics played a major role in sustaining microbial growth in low nutrient conditions and had an important control over the N cycle. The reaction network and model structure presented in this study provide a tool to analyze and predict the long-term nutrient dynamics of both natural and engineered aquatic ecosystems.

1. Introduction

Suspended particulate matter (SPM) has emerged as an important area of study for its role in geomorphology of coastal areas, estuaries, river banks, waterways, and harbors (e.g., Siviglia & Crosato, 2016; Toffolon, 2002) and in changing the quality of water and deposits (e.g., Bilotta & Brazier, 2008; Golterman et al., 1983; McCready et al., 2006). Over the years, a solid physical understanding of sediment dynamics has been established to model and predict sediment transport and deposition in natural waters (e.g., Green & Coco, 2014; Kranck, 1973; Maggi, 2005; McCave, 1984). However, this has mainly focused on hydrodynamic processes, with very little attention paid toward biological processes and ecological functions that modulate the dynamics of microbial community growing on suspended and deposited sediment, which, in turn, affects its transport and deposition (e.g., De Brouwer et al., 2000; Grossart et al., 2006; Kiørboe et al., 2002; Maggi, 2009; Montserrat et al., 2008; Tang & Maggi, 2016).

SPM never occurs as solely mineral. Mineral and biological phases normally coexist near-shore and in SPM because exchanges of nutrients, organic carbon, contaminants, and microorganisms between terrestrial and aquatic ecosystems happen at intense rates and high frequencies for multiple hydrometeorological, morphological, and geochemical causes (e.g., Callender & Hammond, 1982; Groffman & Bohlen, 1999; Gu et al., 2012; Wall et al., 2001). High heterogeneity in composition and the complexity of abiotic and biotic processes (e.g., chemicals, nutrients, and oxygen availability) make SPM a highly dynamic habitat capable of supporting a great variety of microbial strains in facilitative (mutualism and commensalism), competitive, or symbiotic interrelationship with one another (e.g., Dang & Lovell, 2016; Groffman & Bohlen, 1999; Horner-Devine et al., 2004); for instance, an oxygen gradient may develop within a SPM aggregate where the surface may be fully oxic and the inner core may be anoxic; hence, implying that both aerobic and anaerobic microorganisms can coexist and be active on the same aggregate (e.g., Ebrahimi & Or, 2015; Madigan et al., 2010). Each microbial population has its own ecological functions in the sedimentary microecosystem, and the interactions between them are complex and largely not understood. For example, phototrophic microalgae are the primary producers in the ecosystem, providing nutrients to heterotrophs (e.g., Brönmark & Hansson, 2005; Duarte & Cebrian, 1996) and oxygen to aerobic microorganisms; they may enhance, for example, mineralization of organic matter and nitrification (e.g., Pind et al., 1997; Rizzo, 1990; Wilson, 2006), which can then result

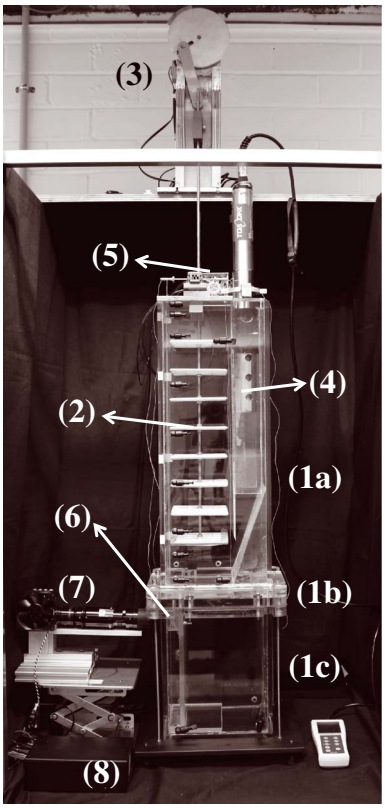

Figure 1. The experimental facility. (1) The settling column with (a) the flocculation section, (b) the diaphragm, and (c) the measuring section; (2) the oscillating grid used to provide isotropic and homogeneous mixing to the suspension; (3) motor and wheel that drive the grid; (4) water quality meter; (5) Cree light-emitting diode used to illuminate settling SPM; (6) optical fibers holder used to enhance illumination; (7) camera and magnification lens used to acquire images of free settling suspended particulate matter; and (8) microcontrolling system used to automate each component of the facility.

in positive feedback on the microalgae. However, how microbial composition changes against a changed environment is a complex problem that has been difficult to explain in its entirety. For instance, microorganisms colonizing and living on SPM (e.g., Grossart et al., 2006; Kiørboe et al., 2002, 2003; Kirchman, 2002) have been found to alter the chemistry, structure, and ambient characteristics of their habitat (e.g., size, surface irregularity, compactness, shear strength, permeability, stability, and sedimentation rate; Jones et al., 1994; Lubarsky et al., 2010; Maggi, 2015b; Maggi & Tang, 2015; Meadows et al., 2012; Tang & Maggi, 2016). Offsets in microbial ecological balance stemming from external perturbations such as changes in water temperature, nutrient concentrations, and presence of contaminants may therefore induce modification to the structure, transport, and deposition of SPM.

The aim of this study is to investigate the extent to which changes in nutrient supply can superpose changes in the native sedimentary microbial community, which in turn controls the N cycle. Focusing on the biogeochemical processes and ecological functions governed by NH_4^+ and NO_3^- leaching, we explore the microbial control on N fluxes and the effects of N leaching and dissolved oxygen on the microbial functional groups responsible for N cycle. Investigations were carried out by integrating experiments with biogeochemical modeling to describe the interactions between mineral, chemical, and biological phases in a sediment suspension. The experiment and model descriptions are presented in section 2, while the analyses of N cycle are presented in section 3.

2. Methods

2.1. Experiments

Three SPM suspension types (nutrient and biomass free NFBF, nutrient affected and biomass free, NABF, and nutrient and biomass affected, NABA) were tested for changes in SPM characteristic and water quality as a result of interactions between nutrients, minerals, and biological processes. While quantification of SPM physical characteristics was previously presented in Tang and Maggi (2016), this study focuses on the nutrient and mineral interactions relative to the NABF and NABA tests.

NABA tests were carried out by inoculating homogenous kaolinite mixtures with microbial strains present in natural sediment collected from the shallow water at the Blackwattle Bay, Sydney, NSW, Australia, on 1 January in 2015. NABA samples were prepared using 500 ml deionized water with added ammonium nitrate NH_4NO_3 and glucose $C_6H_{12}O_6$ as N and C sources at C:N ratio of 5:1. NABA samples were incubated for 21 days at 21°C at room atmosphere. NABF samples were prepared by mixing kaolinite with NH_4NO_3 dissolved in deionized water but were neither inoculated with microbial strains nor incubated. Three kaolinite concentrations C_K and two NH_4NO_3 concentrations were tested for each suspension type.

After incubation, samples were transferred into a settling column filled with 15 L of tap water. The chemical properties of tap water (i.e., NH_4^+, NO_3^-, and Cl^- concentrations, pH, and dissolved O_2) were measured prior to each test. The settling column (Figure 1) was equipped with an oscillating grid system to homogeneously mix the suspension and a water quality monitoring system to measure pH, dissolved O_2, water temperature, turbidity, and NH_4^+, NO_3^-, and Cl^- concentrations every 30 s for approximately 15 hr at 21°C during each test. Detailed description of the settling column and experimental procedures was reported in Tang and Maggi (2015, 2016).

2.2. Reaction Network

Figure 2 shows the NH_4^+ and NO_3^- reaction pathways mediated by microorganisms, their adsorption, aqueous complexation, and gas exsolution. The microbial functional groups, reflecting those living in the estuarine

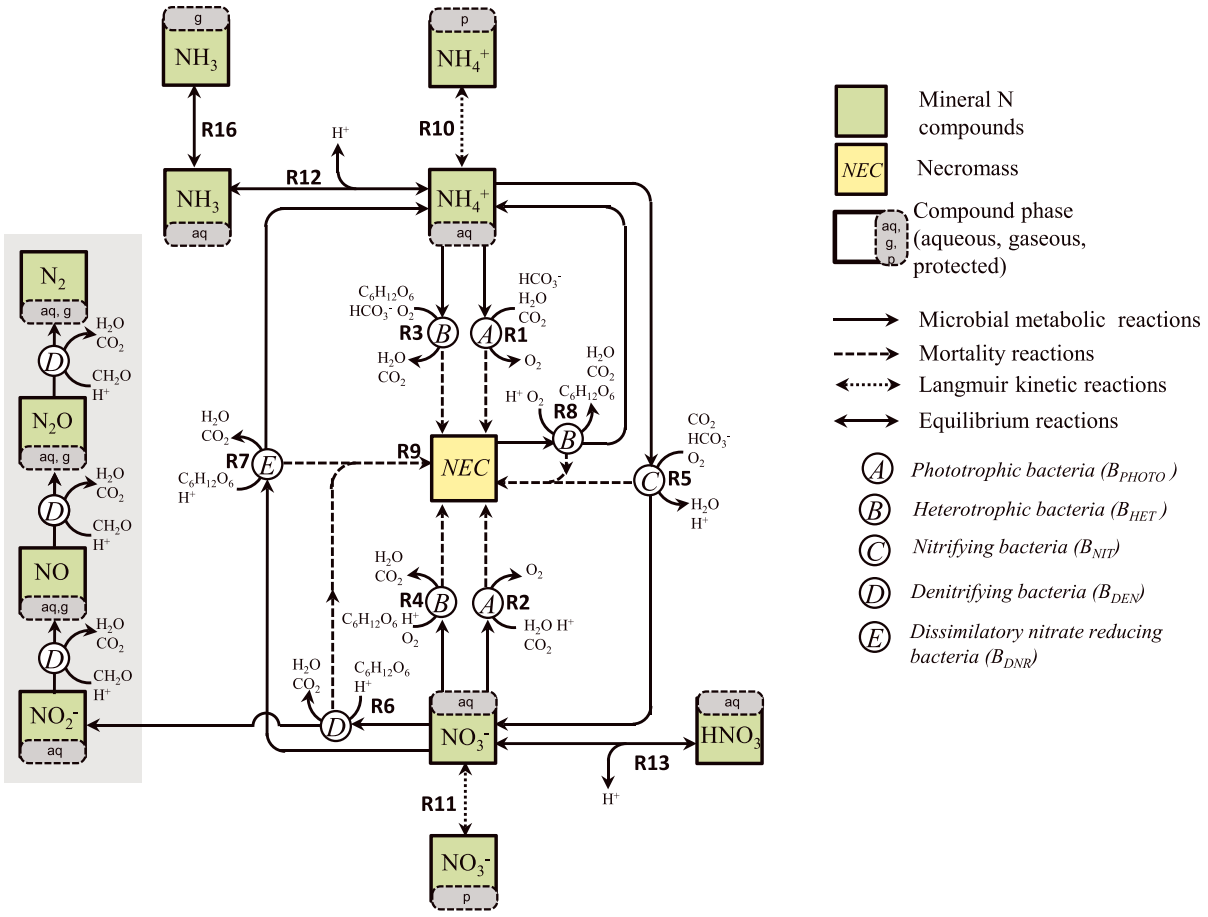

Figure 2. Biogeochemical reaction network of inorganic nitrogen cycle in suspended sediment described in the model. Pathways shaded in grey were not included in the model.

ecosystem, included (i) phototrophic bacteria B_{PHOTO} (e.g., cyanobacteria; Dworkin et al., 2006; Gottschalk, 1986; Raven, 2009); (ii) aerobic heterotrophic bacteria B_{HET} (e.g., pseudomonads and bacilli; *Mesonia*; Gottschalk, 1986; Wilson et al., 2010); (iii) nitrifying bacteria B_{NIT} (e.g., *Nitrosomonas*, *Nitrobacter*; Gottschalk, 1986; Raven, 2009; Van Kessel, 1977); (iv) denitrifying bacteria B_{DEN} (Van Kessel, 1977); and (v) dissimilatory nitrate reducing bacteria B_{DNR} (Van Kessel, 1977). A microbial metabolic reaction R_M was described as the sum of catabolic (energy producing) R_C and anabolic (biomass yielding) R_A reactions as (Rittmann & McCarty, 2001),

$$R_M = (1 - e)R_C + eR_A, \tag{1}$$

where e is the electrons (e^-) fraction used for anabolism, $R_C = R_a - R_d$, and $R_A = R_s - R_d$, with R_a the e^- acceptor half-reaction, R_d the e^- donor half-reaction, and R_s the cell synthesis half-reaction. All microbial functional groups were described by dry mass stoichiometric composition of $C_5H_7O_2N$, though this may differ among microbial strains (e.g., Ebeling et al., 2006; Rittmann & McCarty, 2001).

B_{PHOTO} uses H_2O as e^- donor to produce energy and releases H^+ and O_2 as oxidization products (e.g., Kelly, 1971; Raven, 2009). Energy produced is used to reduce CO_2 (Kelly, 1971) and form glyceraldehyde-3-phosphate, which is used as the building block for cell synthesis (Rittmann & McCarty, 2001) in conjunction with either NH_4^+ or NO_3^- as the N source. The NH_4^+ and NO_3^- phototrophic assimilation (R1 and R2) were written as

$$\text{R1} \quad : \quad e_{R1}NH_4^+ + e_{R1}HCO_3^- + 4e_{R1}CO_2(aq) + e_{R1}H_2O(aq) \quad \rightarrow \quad 5e_{R1}O_2(aq) + e_{R1}B_{PHOTO}$$

$$\text{R2} \quad : \quad \frac{e_{R2}}{3}NO_3^- + \frac{e_{R2}}{3}H^+ + \frac{5e_{R2}}{3}CO_2(aq) + e_{R2}H_2O(aq) \quad \rightarrow \quad \frac{7e_{R2}}{3}O_2(aq) + \frac{e_{R2}}{3}B_{PHOTO}$$

B_{HET} assimilates either NH_4^+ (R3) or NO_3^- (R4) to synthesis biomass by using $C_6H_{12}O_6$ and O_2 as the e^- donor and acceptor, respectively, (Gottschalk, 1986), resulting in

$$\text{R3}: \quad \frac{6e_{R3}}{5}NH_4^+ + C_6H_{12}O_6 + \frac{6e_{R3}}{5}HCO_3^- + 6(1-e_{R3})O_2(aq) \rightarrow \left(6-\frac{24e_{R3}}{5}\right)CO_2(aq) + \left(6-\frac{6e_{R3}}{5}\right)H_2O(aq) + \frac{6e_{R3}}{5}B_{HET}$$

$$\text{R4}: \quad \frac{6e_{R4}}{7}NO_3^- + C_6H_{12}O_6 + \frac{6e_{R4}}{7}H^+ + 6(1-e_{R4})O_2(aq) \rightarrow \left(6-\frac{30e_{R4}}{7}\right)CO_2(aq) + \left(6-\frac{18e_{R4}}{7}\right)H_2O(aq) + \frac{6e_{R4}}{7}B_{HET}$$

B_{NIT} uses O_2 as the e^- acceptor to oxidize NH_4^+ to NO_3^- with a fraction of NH_4^+ being assimilated and CO_2 as the carbon source to build biomass (Ebeling et al., 2006; Rittmann & McCarty, 2001). This metabolic reaction (R5) was written as

$$\text{R5}: \quad \left(1-\frac{e_{R5}}{8}\right)NH_4^+ + e_{R5}CO_2(aq) + \frac{e_{R5}}{4}HCO_3^- + 2(1-e_{R5})O_2(aq) \rightarrow \left(1-\frac{3e_{R5}}{8}\right)NO_3^- + \left(1-\frac{5e_{R5}}{8}\right)H_2O(aq) + \left(2-\frac{3e_{R5}}{4}\right)H^+ + \frac{e_{R5}}{4}B_{NIT}$$

B_{DEN} is responsible for NO_3^- denitrification, whereas B_{DNR} performs dissimilatory NO_3^- reduction (DNR). Both B_{DEN} and B_{DNR} oxidize $C_6H_{12}O_6$ to CO_2 under anaerobic condition with NO_3^- as the e^- acceptor and a fraction of NO_3^- being assimilated. The metabolic reactions for denitrification (R6) and DNR (R7) were expressed as

$$\text{R6}: \quad \left(12-\frac{78e_{R6}}{7}\right)NO_3^- + C_6H_{12}O_6 + \frac{6e_{R6}}{7}H^+ \rightarrow 12(1-e_{R6})NO_2^- + \left(6-\frac{30e_{R6}}{7}\right)CO_2(aq) + \left(6-\frac{18e_{R6}}{7}\right)H_2O(aq) + \frac{6e_{R6}}{7}B_{DEN}$$

$$\text{R7}: \quad \left(3-\frac{15e_{R7}}{7}\right)NO_3^- + C_6H_{12}O_6 + \left(6-\frac{36e_{R7}}{7}\right)H^+ \rightarrow 3(1-e_{R7})NH_4^+ + \left(6-\frac{30e_{R7}}{7}\right)CO_2(aq) + \left(3+\frac{3e_{R7}}{7}\right)H_2O(aq) + \frac{6e_{R7}}{7}B_{DNR}$$

All functional groups are assumed to perish (R9) into biodegradable necromass (NEC) defined by the same chemical formula as living microorganisms ($C_5H_7O_2N$). NEC is then aerobically ammonified and depolymerized to NH_4^+ and $C_6H_{12}O_6$ (R8) by B_{HET} as (e.g., Canfield et al., 2005; Riley et al., 2014)

$$\text{R8}: \quad 2NEC + \frac{(23-11e_{R8})}{4}O_2(aq) + 5H^+ \rightarrow (2-e_{R8})NH_4^+ + (5-3e_{R8})CO_2(aq) + \frac{1+e_{R8}}{2}H_2O(aq) + \frac{5-2e_{R8}}{6}C_6H_{12}O_6 + e_{R8}B_{HET}$$

Finally, NH_4^+ and NO_3^- protection onto minerals (R10 and R11) as a result of adsorption, ion exchange, physical protection in mineral and organic matrix, and other uncharacterized processes (Riley et al., 2014) is considered to be not accessible for microbial consumption (Knicker & Hatcher, 1997). NH_4^+ and NO_3^- are also considered to be in equilibrium with $NH_3(aq)$ and $HNO_3(aq)$ (R12 and R13), whereas $NH_3(g)$, $O_2(g)$, and $CO_2(g)$ dissolution reactions (R16 to R18) are also accounted for explicitly. Derivations of Redox metabolic reactions R1 to R7 are reported in supporting information, and the kinetic parameters for reactions R9 to R18 are listed in Table 1.

2.3. Biogeochemical Modeling

The reaction network in Figure 2 was solved in the general purpose multiphase and multicomponent solver BRTSim-v2 based on Maggi (2015a). Equilibrium aqueous complexation and gaseous dissolution reactions were solved using the mass action law,

$$K_\beta = \prod_R [X_R]^{-x_R} \cdot \prod_P [X_P]^{x_P}, \tag{2}$$

Journal of Geophysical Research: Biogeosciences

10.1002/2017JG004165

Table 1
Summary of Microbial Metabolic Reactions, Langmuir Adsorption Kinetic Reactions, and Equilibrium Aqueous Complexation and Gas Dissolution Reactions Included in the Reaction Network

Microbial metabolic kinetic reactions		Electron donor	Electron acceptor	Respiration type	Carbon source
R1	$\frac{1}{2}e_{R1}NH_4^+ + 2e_{R1}H^+ + \frac{5}{2}e_{R1}HCO_3^- \rightarrow \frac{5}{2}e_{R1}O_2(aq) + \frac{3}{2}e_{R1}H_2O(aq) + \frac{1}{2}e_{R1}B_{PHOTO}$	H_2O	CO_2	Aerobic	CO_2
R2	$\frac{5}{14}e_{R2}NO_3^- + \frac{15}{7}e_{R2}H^+ + \frac{25}{14}e_{R2}HCO_3^- \rightarrow \frac{5}{2}e_{R2}O_2(aq) + \frac{5}{7}e_{R2}H_2O(aq) + \frac{5}{14}e_{R2}B_{PHOTO}$	H_2O	CO_2	Aerobic	CO_2
R3	$\frac{6}{5}e_{R3}NH_4^+ + C_6H_{12}O_6 + 6(1-e_{R3})O_2(aq) \rightarrow (6-\frac{24}{5}e_{R3})H^+ + (6-6e_{R3})HCO_3^- + \frac{18}{5}e_{R3}H_2O(aq) + \frac{6}{5}e_{R3}B_{HET}$	$C_6H_{12}O_6$	O_2	Aerobic	$C_6H_{12}O_6$
R4	$\frac{6}{7}e_{R4}NO_3^- + C_6H_{12}O_6 + 6(1-e_{R4})O_2(aq) \rightarrow (6-\frac{36}{7}e_{R4})H^+ + (6-\frac{30}{7}e_{R4})HCO_3^- + \frac{12}{7}e_{R4}H_2O(aq) + \frac{6}{7}e_{R4}B_{HET}$	$C_6H_{12}O_6$	O_2	Aerobic	$C_6H_{12}O_6$
R5	$(1-\frac{1}{8}e_{R5})NH_4^+ + 2(1-e_{R5})O_2(aq) + \frac{5}{4}e_{R5}HCO_3^- \rightarrow (1-\frac{3}{8}e_{R5})NO_3^- + (2-\frac{7}{4}e_{R5})H^+ + (1+\frac{3}{8}e_{R5})H_2O(aq) + \frac{1}{4}e_{R5}B_{NIT}$	NH_4^+	O_2	Aerobic	CO_2
R6	$(12-\frac{78}{7}e_{R6})NO_3^- + C_6H_{12}O_6 \rightarrow 12(1-e_{R6})NO_2^- + (6-\frac{36}{7}e_{R6})H^+ + (6-\frac{30}{7}e_{R6})HCO_3^- + \frac{12}{7}e_{R6}H_2O(aq) + \frac{6}{7}e_{R6}B_{DEN}$	$C_6H_{12}O_6$	NO_3^-	Anaerobic	$C_6H_{12}O_6$
R7	$(3-\frac{15}{7}e_{R7})NO_3^- + C_6H_{12}O_6 \rightarrow 3(1-e_{R7})NH_4^+ + \frac{6}{7}e_{R7}H^+ + (6-\frac{30}{7}e_{R7})HCO_3^- + (\frac{33}{7}e_{R7}-3)H_2O(aq) + \frac{6}{7}e_{R7}B_{DNR}$	$C_6H_{12}O_6$	NO_3^-	Anaerobic	$C_6H_{12}O_6$
R8	$2NEC + \frac{(23-11e_{R8})}{4}O_2(aq) + 3e_{R8}H^+ + (\frac{9}{2}-\frac{7}{2}e_{R8})H_2O(aq) \rightarrow (2-e_{R8})NH_4^+ + (5-3e_{R8})HCO_3^- + \frac{(5-2e_{R8})}{6}C_6H_{12}O_6 + e_{R8}B_{HET}$	NEC	O_2	Aerobic	NEC
Microbial mortality reaction		δ (s^{-1})			
R9	$B_x \rightarrow NEC$	2×10^{-6}[a]			
Langmuir adsorption kinetic reactions		K_L (L/mol)	q_m (mol/g)	q_0 (mol/g)	
R10	$NH_4^+(aq) \leftrightarrow NH_4^+(p)$	443.3[b]	1.07×10^{-3}[b]	1.06×10^{-4}[b]	
R11	$NO_3^-(aq) \leftrightarrow NO_3^-(p)$	1608.4[b]	1.45×10^{-3}[b]	3.41×10^{-9}[b]	
Equilibrium aqueous complexation reactions		$\log(K_{(aq)})$ at 25°C	$\log(K_{(aq)})$ at 21°C		
R12	$NH_4^+ \leftrightarrow H^+ + NH_3(aq)$	−9.24[c]	−9.37[d]		
R13	$HNO_3(aq) \leftrightarrow H^+ + NO_3^-$	1.30[c]	1.35[d]		
R14	$OH^- + H^+ \leftrightarrow H_2O(aq)$	13.99[c]	14.13[d]		
R15	$CO_2(aq) + H_2O(aq) \leftrightarrow H^+ + HCO_3^-$	−6.34[c]	−6.37[d]		
Equilibrium gas dissolution reactions		$\log(K_{(g)})$ at 25°C	$\log(K_{(g)})$ at 21°C		
R16	$NH_3(g) \leftrightarrow NH_3(aq)$	1.80[c]	1.88[d]		
R17	$O_2(aq) \leftrightarrow O_2(g)$	2.90[c]	2.87[d]		
R18	$CO_2(g) + H_2O(aq) \leftrightarrow H^+ + HCO_3^-$	−7.81[c]	−7.78[d]		

Note. R1 to R8 were written in the form used to code in the BRTSim-v2 solver.
[a]Parameter assumed after Servais et al. (1985) and Billen et al. (1990). [b]Parameters calibrated based on nutrient-affected and biomass-free experiments. [c]Parameters from EQ3/6 at 25°C (Wolery, 1992). [d]Interpolated parameters at 21°C.

where K_β is the equilibrium constant in phase β (either aqueous or gaseous) reported in the EQ3/6 database (Wolery, 1992), $[X_R]$ and $[X_P]$ are the concentrations [mol/L] (for aqueous phase) or partial pressure fraction [−] (for gaseous phase) of reactants X_R and products X_P, respectively, while, x_R and x_P are their corresponding stoichiometric numbers.

NH_4^+ and NO_3^- protection was described using Langmuir adsorption kinetics (e.g., Atkins & De Paula, 2005; Langmuir, 1918) as

$$\frac{d[X(p)]}{dt} = k_a[X(aq)](Q_m - [X(p)]) - k_d[X(p)], \tag{3}$$

where [X(p)] and [X(aq)] are the concentrations [mol/L] of chemical X in protected (p) and aqueous (aq) phases, respectively, k_a and k_d are the adsorption and desorption rate constants, respectively, and $Q_m = q_m C_K$ includes the maximum adsorption capacity q_m [mol of X adsorbed/g of mineral] and the mineral concentration C_K [g/L]. Note that at equilibrium ($d[X(p)]/dt = 0$), $K_L = k_a/k_d = [X(p)]/([X(aq)](Q_m - [X(p)]))$ is the Langmuir equilibrium constant.

Microbial metabolism was described by Michaelis-Menten-Monod kinetics with reaction rate r written as (Maggi, 2015a)

$$r = \hat{\mu} \cdot \frac{[B_x]}{Y} \cdot \prod_p [X_p]^{n_p} \cdot \prod_i \frac{[X_i]}{[X_i] + K_{M_i}\left(1 + \sum_j \frac{[X_j]}{K_{M_j}}\right)} \cdot \prod_m \frac{K_{H_m}}{K_{H_m} + [X_m]}, \tag{4}$$

where $\hat{\mu}$ is the maximum specific biomass growth rate, $[B_x]$ is the concentration of microbial functional group B_x, and Y is the biomass yield. The third factor on the right-hand side describes the n_p-order kinetic product for reactant X_p and $n_p = \{1, 2, 3, \ldots, n\}$ for first, second, third, and n-order kinetics, respectively. The fourth factor on the right-hand side expresses the Michaelis-Menten-Monod kinetic terms for reactant X_i with K_{M_i} its half-saturation concentration. The term in the parenthesis describes the competitive substrate consumption between reactants X_i and X_j with K_{M_j} its half-saturation concentration. The last term on the right-hand side expresses a decrease in r due to the presence of an inhibitor X_m with inhibition constant K_{H_m}. The rate of change in the concentration of a generic chemical X_n was then written as

$$\frac{d[X_n]}{dt} = \sum_i (x_{n_i} \cdot r_i), \tag{5}$$

with x_{n_i} as the stoichiometric number of X_n in reaction r_i. The rate of change in $[B_x]$ was described by Monod kinetics as (Monod, 1949),

$$\frac{d[B_x]}{dt} = \sum_i Y_i r_i - \delta[B_x], \tag{6}$$

where the microbial mortality rate $\delta = 2 \times 10^{-6}$ s^{-1} was assumed after Servais et al. (1985) and Billen et al. (1990) for all functional groups.

Microbial competition for the same substrate was accounted for by K_M in equation (4). All reactions involving O_2(aq) and HCO_3^- consumption were assumed to have the same K_M values. Competitive substrate consumption relative to NH_4^+ and NO_3^- was included for N assimilation by B_{PHOTO} and B_{HET} (R1 to R4). pH inhibition was explicitly accounted for with $K_M = 1 \times 10^{-9}$ mol/L for low $[H^+]$ and with $K_H = 1 \times 10^{-5}$ mol/L for high $[H^+]$ (Boon & Laudelout, 1962; Saleh-Lakha et al., 2009). O_2 inhibition on anaerobic reactions (R6 and R7) was also explicitly included. Finally, $C_6H_{12}O_6$ inhibition on depolymerization and ammonification (R8) was considered here because B_{HET} is expected to have higher preference for simple (i.e., $C_6H_{12}O_6$) over complex C sources such as necromass (Goldman & Dennett, 1991).

2.4. Parameter Estimation

Langmuir kinetic parameters k_a, k_d, and q_m in equation (3), and the initial N ions protected in one gram of minerals q_0 were calibrated for NH_4^+ and NO_3^- adsorption against NABF experiments. The remaining unknowns (i.e., $\hat{\mu}_s$, K_M, K_H, e, and initial biomass concentrations $[B_x]_0$) were estimated against NABA experiment conducted at $[NH_4NO_3]$ = 6 mM, $[C_6H_{12}O_6]$ = 11.6 mM, and $C_K = 3$ g/L; in total, 192 data points of NH_4^+, NO_3^-, pH, and O_2(aq) acquired during the column testing were used for calibration. Model parameters were estimated with Model-Independent Parameter Estimation and Uncertainty Analysis (Doherty, 2005), which uses the Gauss-Marquardt-Levenberg algorithm (Levenberg, 1944) to minimize the errors between modeled and observed data.

The model structure and estimated parameters were validated against independent NABA experiments with [NH_4NO_3], [$C_6H_{12}O_6$] and C_K different from those for estimation. Goodness of fit was measured using the correlation coefficient (R), the normalized root-mean-square error (NRMSE), Nash-Sutcliffe efficiency (NSE) (Nash & Sutcliffe, 1970), index of agreement (IA) (e.g., Willmott, 1982; Willmott et al., 1985), and percent bias (PBIAS) (Sorooshian et al., 1993),

$$R = \frac{\mathrm{cov}(c,o)}{\sigma_c \sigma_o}, \qquad \text{with} \quad -1 \le R \le 1, \tag{7a}$$

$$\mathrm{NRMSE} = \frac{\sqrt{\frac{1}{n_o}\sum_{i=1}^{n_o}(c_i - o_i)^2}}{\max\{o\} - \min\{o\}} \times 100, \qquad \text{with} \quad 0 \le \mathrm{NRMSE} < \infty, \tag{7b}$$

$$\mathrm{NSE} = 1 - \frac{\sum_{i=1}^{n_o}(o_i - c_i)^2}{\sum_{i=1}^{n_o}(o_i - \bar{o})^2}, \qquad \text{with} \quad -\infty < \mathrm{NSE} \le 1, \tag{7c}$$

$$\mathrm{IA} = 1 - \frac{\sum_{i=1}^{n_o}(o_i - c_i)^2}{\sum_{i=1}^{n_o}(|c_i - \bar{o}| + |o_i - \bar{o}|)^2}, \qquad \text{with} \quad 0 \le \mathrm{IA} \le 1, \tag{7d}$$

$$\mathrm{PBIAS} = \frac{\sum_{i=1}^{n_o}(c_i - o_i)}{\sum_{i=1}^{n_o} o_i} \times 100, \qquad \text{with} \quad -\infty < \mathrm{PBIAS} < \infty, \tag{7e}$$

where c and o are the calculated and observed values of the state variables, respectively, n_o is the number of observations, σ_c and σ_o are the corresponding standard deviations, and $\bar{o}$ is the average of o. Modeled values match observations when $R \to 1$, NRMSE$\to$ 0%, NSE$\to$ 1, IA$\to$ 1, and PBIAS $\to$ 0%. NSE = 0 implies that c is as accurate as $\bar{o}$, while, NSE < 0 signifies that $\bar{o}$ is a better prediction than the model. PBIAS measures model overestimation (PBIAS > 0) or underestimation (PBIAS < 0). A validation test was considered satisfactory if conditions $R \ge 0.8$, NRMSE $\le$ 15%, NSE ≥ 0, IA ≥ 0.8, and $-15\% \le$ PBIAS $\le 15\%$ were satisfied and signified that model structure and parameter uncertainty were suitable to describe that experiment.

2.5. Analyses of Nutrient Leaching and Dissolved Oxygen Content

The model was used to investigate the effects of NH_4^+ and NO_3^- leaching on microbial dynamics at steady state. A total of 400 simulations were run for leaching rates $R_{NH_4^+}$ and $R_{NO_3^-}$ between 5×10^{-4} and 5×10^{-2} mol $\cdot$ L^{-1} $\cdot$ day^{-1}. All simulations were initialized with equal biomass across all functional groups. C:N ratio was kept at 8:1 as commonly found in estuarine sediment (Matson & Brinson, 1990), while C_K was kept at 0.1 g/L. Microbial metabolism was assumed not to be limited by [H^+], [HCO_3^-], and [O_2(aq)], which were assumed to be continuously recharged in natural aquatic ecosystem through various buffering processes not explicitly included in the model; hence, pH was kept at approximately 7 and [HCO_3^-] was maintained at approximately 6×10^{-5} mol/L so as to be in equilibrium with pH 7 and atmospheric CO_2(g). The concentration of dissolved oxygen was maintained at 2.87×10^{-4} mol/L, which corresponds to 100% saturation at 21°C. Simulations were run until the ecosystem reached the steady state.

Simulations of $R_{NH_4^+}$ and $R_{NO_3^-}$ between 5×10^{-4} and 5×10^{-2} mol $\cdot$ L^{-1} $\cdot$ day^{-1} with $R_{NH_4^+}$:$R_{NO_3^-}$ = 1:1 were also conducted at different O_2(aq) saturations to investigate the effects of O_2 on N fluxes. All simulations were conducted with the same boundary and initial conditions as above.

3. Results

3.1. Analysis of Kinetic Parameters

Estimated Langmuir parameters for NH_4^+ and NO_3^- adsorption on kaolinite (Table 1) matched relatively well those reported in the literature (e.g., Cengeloglu et al., 2006; Copcia et al., 2010; Li & Bowman, 2001). Experimentally determined kinetic parameters relative to reactions R1 to R8 are listed in Table 2. The maximum specific biomass growth rate $\hat{\mu}$ ranged from about 1×10^{-5} (R3) to 4×10^{-4} s^{-1} (R8). The biomass yield Y was the highest in phototrophic NH_4^+ assimilation in R1 and nitrification in R5 and the lowest in necromass depolymerization in R8. No correlation was found between $\hat{\mu}$ and Y (i.e., $R = -0.46$). K_M values spanned across a wide range from 1.5×10^{-6} to 5.7×10^{-2} mol/L (Table 2). The O_2(aq) inhibition constant K_H in denitrification in R6 was higher than in DNR in R7, implying that B_{DEN} had higher tolerance to O_2(aq) than B_{DNR}. The reaction

Journal of Geophysical Research: Biogeosciences

10.1002/2017JG004165

Table 2
Summary of Estimated Parameters for Microbial Metabolic Reactions R1 to R8

		Reactions							
Parameter values		R1	R2	R3	R4	R5	R6	R7	R8
Maximum specific biomass growth rate $\hat{\mu}$ ($\times 10^{-5}$ s^{-1})		2.661	10.794	1.000	12.480	16.491	5.573	4.352	40.778
Fraction of electron used for cell synthesis e (-)		1.0	1.0	0.115	0.081	0.149	0.119	0.119	0.046
Biomass yield Y (mol of B_x/mol of C source)		0.25	0.20	0.138	0.069	0.25	0.102	0.102	0.023
Biomass yield Y (g of dry B_x/g of C source)		0.6422	0.5138	0.0866	0.044	0.6422	0.064	0.064	0.023
Michaelis-Menten constant K_M (mol/L)	NH_4^+	3.007×10^{-3}[a]	—	1.405×10^{-5}[b]	—	3.554×10^{-2}	—	—	—
	NO_3^-	—	5.288×10^{-2}[a]	—	1.281×10^{-2}[b]	—	4.636×10^{-3}	6.153×10^{-4}	—
	$C_6H_{12}O_6$	—	—	5.719×10^{-2}[c]	5.162×10^{-3}[c]	—	1.470×10^{-3}	8.096×10^{-4}	—
	O_2(aq)	—	—	6.567×10^{-5}	6.567×10^{-5}	6.567×10^{-5}	—	—	6.567×10^{-5}
	HCO_3^-	1.971×10^{-5}	1.971×10^{-5}	–	—	1.971×10^{-5}	—	—	—
	NEC	—	—	—	—	—	—	—	1.507×10^{-6}
	H^+	1×10^{-9}	1×10^{-9}	1×10^{-9}	1×10^{-9}	1×10^{-9}	1×10^{-9}	1×10^{-9}	1×10^{-9}
Inhibition constant K_H (mol/L)	H^+	1×10^{-5}	1×10^{-5}	1×10^{-5}	1×10^{-5}	1×10^{-5}	1×10^{-5}	1×10^{-5}	1×10^{-5}
	O_2(aq)	—	—	—	—	—	1.907×10^{-3}	1.510×10^{-4}	—
	$C_6H_{12}O_6$	—	—	—	—	—	—	—	6.175×10^{-5}

[a]Competition term was included in R1 and R2 to account for competitive substrate consumption between NH_4^+ and NO_3^-. [b]Competition term was included in R3 and R4 to account for competitive substrate consumption between NH_4^+ and NO_3^-. [c]Competition term was included in R3 and R4 to account for competitive substrate consumption of $C_6H_{12}O_6$.

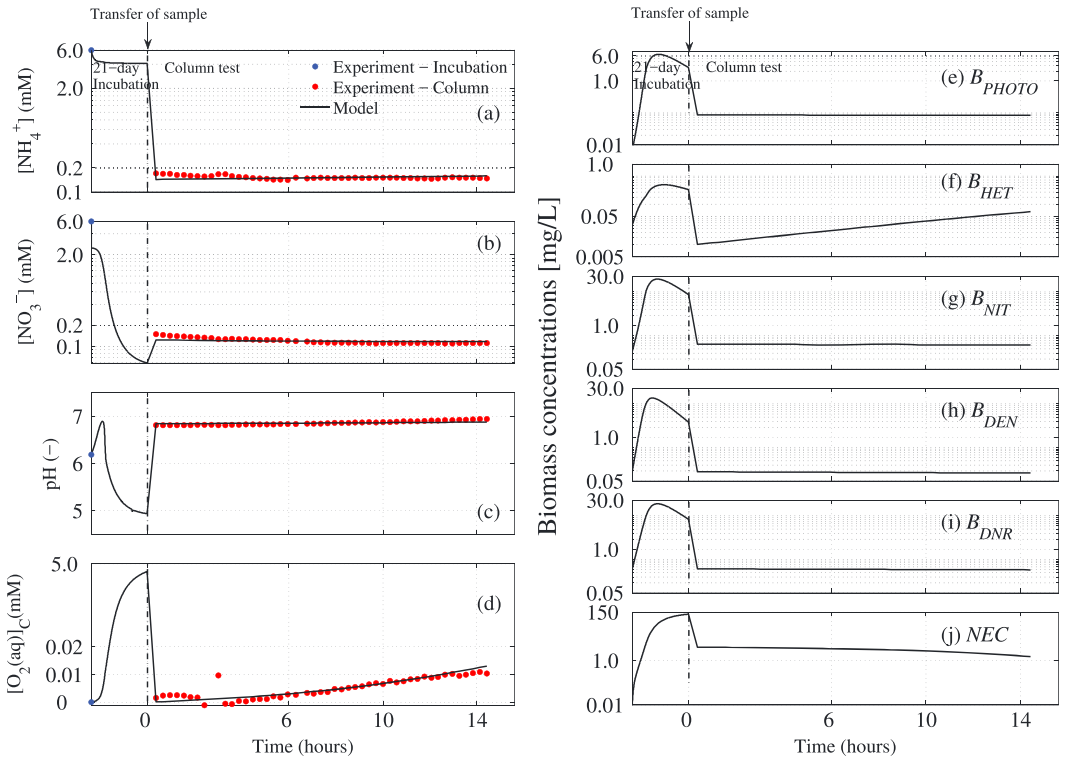

Figure 3. Comparison between experimental measurements and modeled results for (a) $[NH_4^+]$, (b) $[NO_3^-]$, (c) pH, (d) the net oxygen consumption $[O_2(aq)]_C$, and microbial concentrations for (f) phototrophic bacteria B_{PHOTO}, (g) heterotrophic bacteria B_{HET}, (h) nitrifying bacteria B_{NIT}, (i) denitrifying bacteria B_{DEN}, (j) dissimilatory nitrate reducing bacteria B_{DNR}, and (k) necromass (NEC). Note that the incubation phase was plotted in a time scale of days, while the column testing phase was plotted in a time scale of hours.

velocity of R8 was reduced by more than 50% when $[C_6H_{12}O_6] > 6.18 \times 10^{-5}$ mol/L, thus accounting for B_{HET} to have higher preference for simpler monosaccharide as a C source than NEC.

Qualitatively, the model matched relatively well the $[NH_4^+]$, $[NO_3^-]$, pH, and the net O_2 consumption $[O_2(aq)]_C$ measured during column testing (Figure 3, first column). During the 21 day incubation, $[NH_4^+]$ initially decreased due to adsorption onto kaolinite and was nearly constant afterward because NH_4^+ consumed by B_{NIT} in R5 (contributing about 99%) was balanced by its production in reactions R7 and R8 (contributing about 98% and 2%, respectively; Figure 3a). NO_3^- decreased sharply at the beginning of incubation due to adsorption and gradually later on because of consumption by B_{DEN} (68%), B_{DNR} (32%), and B_{HET} and B_{PHOTO} (contributing less than 0.02%) (Figure 3b). NO_3^- produced by B_{NIT} was unable to sustain uptake by other microbial functional groups. After the initial phase, pH stabilized at about 5 by the end of incubation (Figure 3c). The net oxygen consumption $[O_2(aq)]_C$ increased during incubation, implying that the ecosystem had more intense aerobic respiration than photosynthesis (Figure 3d).

All microbial functional groups showed an initial increase in their concentrations (Figure 3, right column) and reached a maximum between day 7 and 14 of the incubation period. In contrast, [NEC] increased steadily. The biomass fraction in each functional group fluctuated during the whole test depending on substrate availability and environmental conditions (e.g., pH, $O_2(aq)$).

3.2. Goodness-of-Fit Analyses

Analyses of goodness of fit show that the modeled concentrations in Figure 3 matched relatively well the experimental $[NH_4^+]$, $[NO_3^-]$, pH, and $[O_2(aq)]_C$, with $R \geq 0.9$, NRMSE $\leq$ 14%, NSE $\geq$ 0.8, IA $\geq$ 0.95, and $-0.5\% \leq$ PBIAS $\leq$ 4% (Figure 4, cells marked with red asterisk).

Validation tests conducted against independent experiments at different $[NH_4NO_3]$ and C_K (Figure 4) also showed relatively good agreement, with 100% state variables having $R \geq 0.8$, 95% having NRMSE $\leq$ 15%,

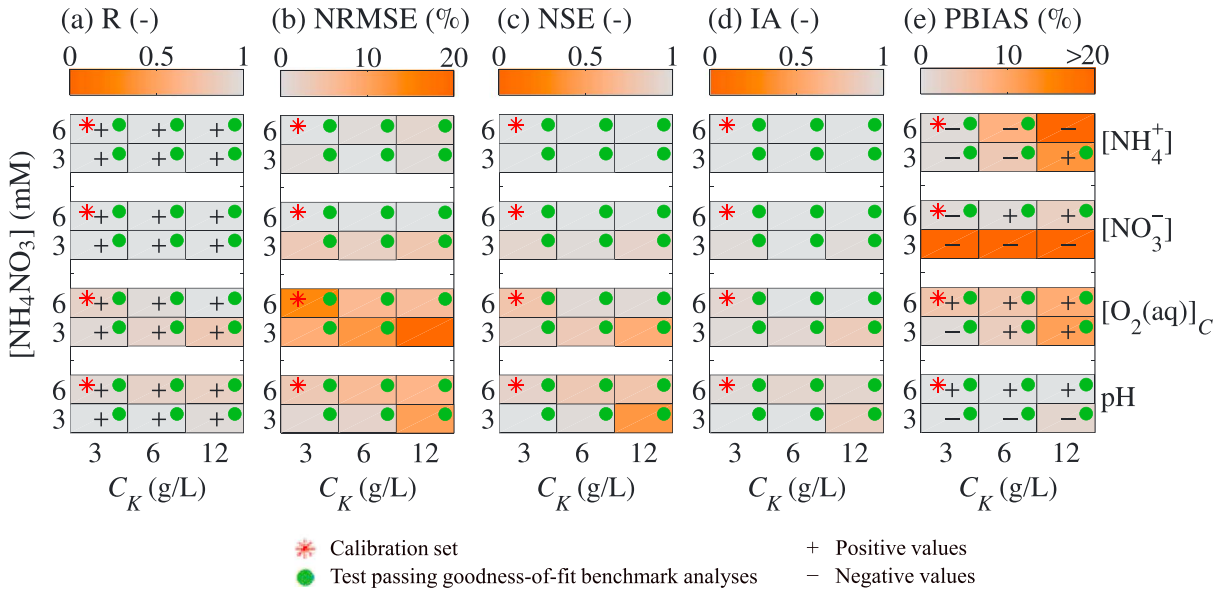

Figure 4. Goodness-of-fit analyses of the modeled against experimental $[NH_4^+]$, $[NO_3^-]$, pH, and the net oxygen consumption $[O_2(aq)]_C$ using (a) correlation coefficient (R), (b) normalized root-mean-square error (NRMSE), (c) Nash-Sutcliffe efficiency (NSE), (d) index of agreement (IA), and (e) percent bias (PBIAS). The red asterisk indicates calibration set and the green dot represents validation tests that passed the goodness-of-fit benchmark analyses. "+" and "−" signs indicate positive and negative values in R and PBIAS tests, respectively. Note that kaolinite concentration C_K and $[NH_4NO_3]$ values plotted correspond to the initial concentrations in incubation.

100% having NSE ≥ 0, 100% having IA ≤ 0.8, and 80% having −15% ≤ PBIAS ≤ 15%; in average, 95% of validation tests passed the benchmark values stated in section 2.4.

3.3. Effect of Nutrient Leaching

The effect of nutrient leaching on the steady state N dynamics and microbial community was investigated using model parameters reported in section 3.1 with pH, $[O_2(aq)]$, and $[CO_2(aq)]$ kept constant at optimum values for microbial growth.

At steady state, the total living biomass B_{TOT} generally increased with increasing $R_{NO_3^-}$, but it decreased when $R_{NH_4^+}$ was greater than 2×10^{-2} mol · L^{-1} · day^{-1} (Figure 5a). In contrast, the necromass NEC (not shown here) increased linearly with increasing nutrient leaching rates. Among all microbial groups, B_{PHOTO} constituted 92% of B_{TOT} (Figure 5b), while B_{HET} contributed less than 8% at $R_{NH_4^+} < 2 \times 10^{-2}$ mol/L (Figure 5c) and B_{DNR} survived only when leaching rates were greater than 2×10^{-2} mol · L^{-1} · day^{-1} (Figure 5d). B_{NIT} and B_{DEN} were completely outcompeted by the other functional groups at steady state, as opposed to the transient incubation phase (Figures 3g and 3h) where they were the most abundant.

In all nutrient leaching scenarios, more than 99% of N was immobilized into biomass, less than 1% remained in the aqueous phase, and less than 0.03% was protected in minerals. The total N mass flow through each

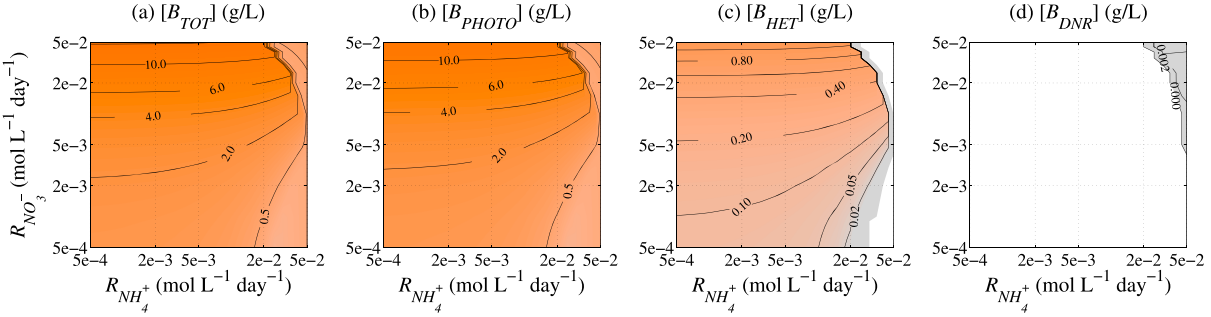

Figure 5. Concentrations of (a) total living biomass B_{TOT}, (b) phototrophic bacteria B_{PHOTO}, (c) heterotrophic bacteria B_{HET}, and (d) dissimilatory nitrate reducing bacteria B_{DNR} at steady state and for leaching rates $R_{NH_4^+}$ and $R_{NO_3^-}$ ranging between 5×10^{-4} and 5×10^{-2} mol · L^{-1} · day^{-1}. The white areas indicate that the microbial concentration is 0.

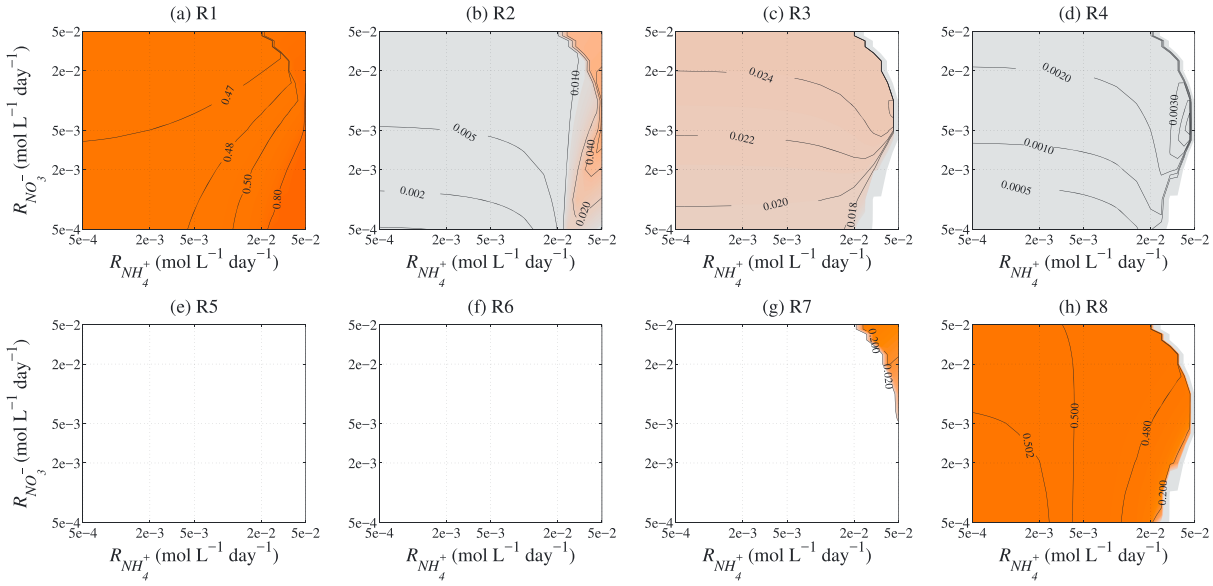

Figure 6. Mass fraction of N consumed in (a) phototrophic NH_4^+ assimilation R1, (b) phototrophic NO_3^- assimilation R2, (c) heterotrophic NH_4^+ assimilation R3, (d) heterotrophic NO_3^- assimilation R4, (e) nitrification R5, (f) denitrification R6, (g) dissimilatory nitrate reduction R7, and (h) necromass depolymerization and ammonification R8 at steady state and for leaching rates $R_{NH_4^+}$ and $R_{NO_3^-}$ ranging between 5×10^{-4} and 5×10^{-2} mol · L^{-1} · day^{-1}. Note that the contours have values ranging between 0 and 1. The white areas indicate that the N fraction is 0.

microbial reaction at steady state is depicted in Figure 6. The majority of total N was consumed by B_{PHOTO} and B_{HET} through phototrophic NH_4^+ assimilation in R1 and NEC depolymerization and ammonification in R8, respectively (Figures 6a and 6h). Mineralization of NEC to NH_4^+ facilitated growth of B_{PHOTO} and B_{HET}, which later contributed to the increase in NEC, therefore resulting in a positive feedback that enabled the ecosystem to self-sustain even in scenarios where nutrient inputs were low. Our analysis shows that NEC depolymerization released NH_4^+ at a high rate (approximately 2×10^{-2} · mol · L^{-1} · day^{-1}) in scenarios with low nutrient leaching and was a major contributor to the microbial growth. At high nutrient leaching, inhibition of NEC depolymerization by high availability of $C_6H_{12}O_6$ lowered the concentration of NH_4^+ available to microbial growth, thus resulting in decreased [B_{TOT}] (Figure 5a). Overall, our results show that NEC depolymerization had a very important contribution to the N cycle.

Analysis in Figure 6 shows that B_{PHOTO} had a higher preference for NH_4^+ over NO_3^- and was mainly synthesized through R1, in line with earlier observations (e.g., Caperon & Meyer, 1972; Cochlan & Harrison, 1991; McCarthy et al., 1977). Although NEC depolymerization played an important role in the N mass flow, B_{HET} synthesized from NEC had lower concentration than that produced by R3 because of smaller biomass yield Y in R8 than in R3 (Table 2). B_{HET} also showed a higher preference for NH_4^+ over NO_3^-; however, its growth was greatly suppressed by B_{PHOTO} due to high K_M for $C_6H_{12}O_6$. Similar experimental observations were also found

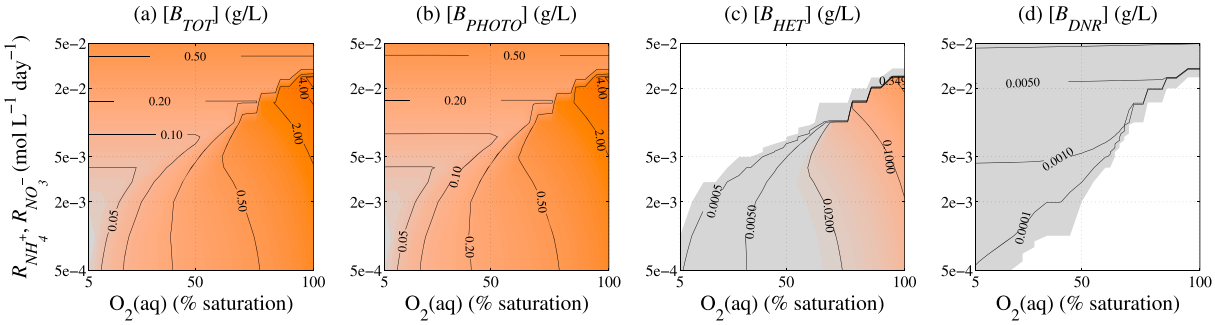

Figure 7. Concentrations of (a) total living biomass B_{TOT}, (b) phototrophic bacteria B_{PHOTO}, (c) heterotrophic bacteria B_{HET}, and (d) dissimilatory nitrate reducing bacteria B_{DNR} at steady state and for leaching rates $R_{NH_4^+}$ and $R_{NO_3^-}$ ranging between 5×10^{-4} and 5×10^{-2} mol · L^{-1} · day^{-1} with $R_{NH_4^+}$:$R_{NO_3^-}$ = 1:1 and for O_2(aq) saturation ranging from 5 to 100%. The white areas indicate that the microbial concentration is 0.

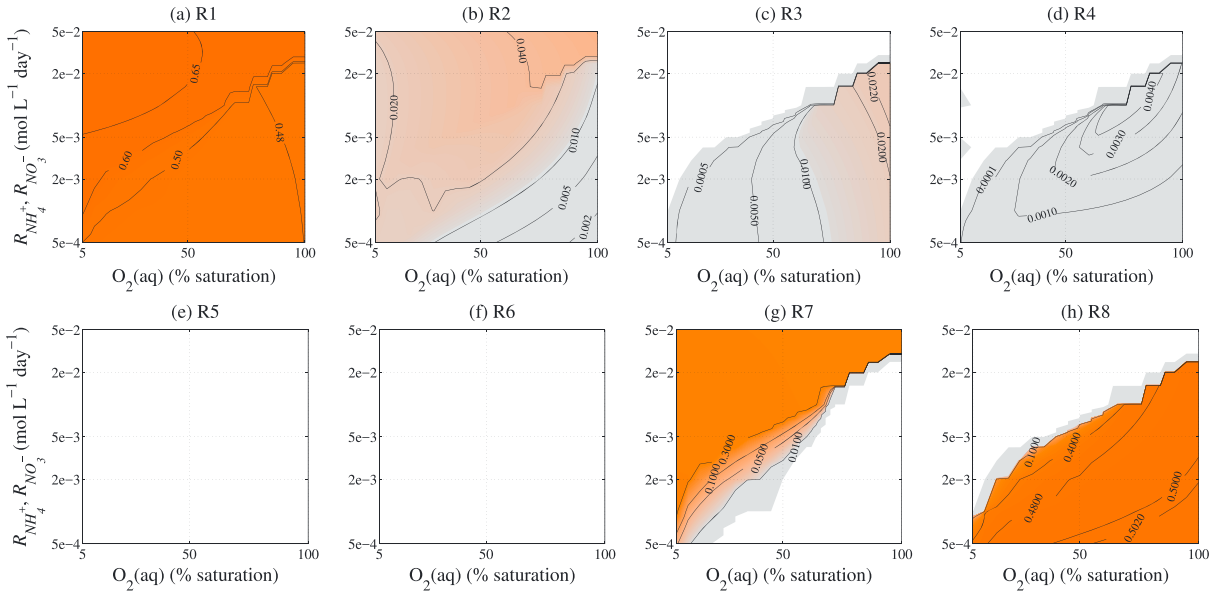

Figure 8. Mass fraction of N consumed in (a) phototrophic NH_4^+ assimilation R1, (b) phototrophic NO_3^- assimilation R2, (c) heterotrophic NH_4^+ assimilation R3, (d) heterotrophic NO_3^- assimilation R4, (e) nitrification R5, (f) denitrification R6, (g) dissimilatory nitrate reduction R7, and (h) necromass depolymerization and ammonification R8 at steady state and for leaching rates $R_{NH_4^+}$ and $R_{NO_3^-}$ ranging between 5×10^{-4} and 5×10^{-2} mol · L^{-1} · day^{-1} with $R_{NH_4^+}$:$R_{NO_3^-}$ = 1:1 and for O_2(aq) saturation ranging from 5 to 100%. Note that the contours have values ranging between 0 and 1. The white areas indicate that the N fraction is 0.

in Tufail (1987) and Kirchman and Wheeler (1998). Although O_2(aq) inhibition on B_{DNR} was higher than B_{DEN}, approximately 30% of total N was partitioned into DNR in R7 at high nutrient leaching rates (Figure 6g) because B_{DNR} had lower K_M for both NO_3^- and $C_6H_{12}O_6$ than B_{DEN}.

3.4. Effect of Dissolved Oxygen Content

The reaction network in Figure 2 consisted of both aerobic and anaerobic metabolic processes, which are sensitive to the concentration of dissolved oxygen. To investigate how microbial dynamics and N fluxes are controlled by [O_2(aq)], simulations were conducted for O_2(aq) saturation ranging from 5 to 100%, and for leaching rates $R_{NH_4^+}$ and $R_{NO_3^-}$ ranging between 5×10^{-4} and 5×10^{-2} mol · L^{-1} · day^{-1} with $R_{NH_4^+} : R_{NO_3^-} = 1 : 1$.

B_{TOT} generally increased with increasing [O_2(aq)], but it was not sensitive to [O_2(aq)] when the leaching rates exceeded 3×10^{-2} · mol · L^{-1} · day^{-1} (Figure 7a). Interestingly, [B_{PHOTO}] was highly correlated to [O_2(aq)] (Figure 7b) even though the growth of B_{PHOTO} did not depend on O_2(aq) as a substrate. This is because the NEC depolymerization in R8 was inhibited by low [O_2(aq)], and therefore NH_4^+ available for consumption by B_{PHOTO} decreased with decreasing [O_2(aq)]. B_{HET} did not survive well in conditions where [O_2(aq)] was below 50% saturation (Figure 7c), whereas, B_{DNR} could survive in anoxic conditions (Figure 7d). In all tested scenarios, B_{NIT} and B_{DEN} were completely outcompeted by other microbial groups at steady state.

The N mass flow through phototrophic NH_4^+ assimilation in R1 generally decreased with increasing O_2(aq) saturation (Figure 8a), while the N fraction consumed by NO_3^- phototrophic assimilation in R2 increased with increasing [O_2(aq)] at high nutrient leaching rates (Figure 8b). A small fraction of N was partitioned into heterotrophic metabolism in R3 and R4 at low leaching rates, while they were not active in low [O_2(aq)] and high leaching rates (Figures 8c and 8d). Approximately 30% of N was consumed by B_{DNR} in R7 in low [O_2(aq)] regardless of leaching rates (Figure 8g). The N fraction consumed in NEC depolymerization in R8 increased with increasing O_2(aq) saturation, but the reactions was inhibited at high nutrient conditions (Figure 8h).

4. Discussion

The microbial functional groups described in the reaction network (Figure 2) included different microbial species that performed similar ecological functions, hence assuming that members of the same group were equipped with the same or similar enzymes for the same metabolic mechanisms; in fact, no significant variation was found in K_M when experiments were conducted with different microbial species of the same functional group (Caperon & Meyer, 1972). Several studies also showed that K_M values may greatly depend

on the ambient nutrient concentrations of the original habitat (e.g., Caperon & Meyer, 1972; MacIsaac & Dugdale, 1969); for instance, phytoplankton populations obtained from eutrophic ecosystems were observed to have much higher K_M values for NO_3^- as compared to those living in oligotrophic ecosystems (MacIsaac & Dugdale, 1969). The microbial communities used to inoculate sediment mixtures in this study were sampled from an estuary that has relatively high $[NH_4^+]$ and $[NO_3^-]$ (approximately 1.2 mM of $[NH_4^+]$ and 6.6 mM of $[NO_3^-]$), and hence, the parameters calibrated here may reflect only the metabolic characteristics of microorganisms adapted to high nutrient concentrations and may not be applicable to ecosystem where nutrients are strongly limiting. Along this line, the capability of microorganisms to adapt to a specific nutrient condition (Eppley & Coatsworth, 1968) was not accounted for in the model, and we assumed that enzymes responsible for metabolism were not altered after long-term presence in such an environment. We note also that nitrification pathway in R5 involves two processes conducted separately by ammonia-oxidizing bacteria and archaea, and nitrite-oxidizing bacteria, which may have different substrate affinities, yields, and sensitivities to environmental conditions such as temperature and oxygen content (e.g., Dang & Chen, 2017; Kits et al., 2017). Because concentration of NO_2^- was not measured, experiments were unable to give sufficient constraint for retrieving the kinetic parameters of these two intermediate processes separately; hence, these two processes (ammonia and nitrite oxidation) were treated here as one reaction mediated by one microbial functional group.

Microorganisms were found to attach on SPM at a few orders of magnitude higher concentration than those living freely in ambient water (e.g., Caron et al., 1986; Turley & Mackie, 1994). These two groups of microorganisms were not differentiated in the mode, and hence, the estimated parameters reflected the combined effects resulting from metabolism of both aggregate-attached and free-living microorganisms; however, we note that aggregate-attached bacteria may have higher enzymatic activity and reaction rate than free-living bacteria as evident in Goulder (1977) and Grossart et al. (2007). Several studies also observed the grazing of aggregate-attached microorganisms by heterotrophic microflagellates and suggested that the abundance of bacteria living attached to SPM was controlled by heterotrophic grazing (e.g., Caron, 1987; Kiørboe et al., 2004). Although we note that antagonistic relationships such as predation, grazing, scavenging, and inhibition by metabolites of other species occur among microbial communities (e.g., Cole, 1982; Guerrero et al., 1986; Pernthaler, 2005), these interactions were not explicitly included in the model; indeed, we assume that these interactions were implicitly accounted for through mortality.

Although microorganisms may grow better in environments where micronutrients are available (MacIsaac & Dugdale, 1969), experiments herein were conducted with only inorganic N (NH_4^+ and NO_3^-) and $C_6H_{12}O_6$ without accounting for other macronutrients and micronutrients. Because sulfur-based compounds were not added to the test samples, chemolithoautotrophic denitrification that uses sulfur as electron donor (Batchelor & Lawrence, 1978) was not included in the reaction network. NO_2^-, on the other hand, was very likely present in the test samples because it is an intermediate product of nitrification in R5 and denitrification in R6. Anaerobic ammonium oxidation (Anammox) that uses NO_2^- as electron acceptor (e.g., Dalsgaard et al., 2005) was, however, not considered in the reaction network because experiments described above were conducted in oxic conditions, while Anammox bacteria has high sensitivity to oxygen inhibition (e.g., Davies et al., 1989; Kalvelage et al., 2011); thus, Anammox was assumed to be negligible in our case. We note also that N_2-fixing microorganisms may have a contribution to the N cycle (e.g., Howarth et al., 1988; Newell et al., 2016); however, N_2 fixation was not measured in our experiments and its effect was not included in the reaction network.

Temperature has been reported in the literature as one of the factors that alters the enzymatic activities of microorganisms (e.g., Maggi & Riley, 2017; Toseland et al., 2013). For instance, microbial affinity for NO_3^- in phototrophic and heterotrophic assimilation was found to decrease with decreasing temperature (Reay et al., 1999), whereas a reduction in ammonia oxidation and denitrification rates were also observed as temperature decreased (e.g., Saleh-Lakha et al., 2009; Tourna et al., 2008; Wang et al., 2015). Apart from biochemical reactions, chemical adsorption on clay is also sensitive to temperature (Almeida et al., 2009). In this study, temperature in both experiments and model was kept constant at 21°C, and hence, the parameters calibrated here reflected only the microbial metabolism and adsorption kinetics specific to that temperature.

The model considered a comprehensive ecological feedback loop that explicitly accounted for the biomass of different functional groups and the necromass, which are not normally included in most aquatic biogeochemical models (Robson, 2014). Some models did consider explicitly the biomass with one or more

functional groups; however, most of these models focused on biogeochemical processes (e.g., Allen & Clarke, 2007; Kaufman & Borrett, 2010) with little emphasis on the dynamics of microbial diversity (e.g., Bruce et al., 2006; Prokopkin et al., 2010). Although the calibrated parameters were specific to the microbial strains and environmental conditions tested here, the reaction network and model structure presented herein provide a modeling framework that could be applied to predict, monitor, and manage water quality and microbial communities, not only in natural aquatic ecosystems but also in engineered environments such as wastewater treatment plants, bioremediation plants, bioreactors, aquaculture farms, and microalgae cultivation plants.

4.1. Conclusions

The role of microorganisms in controlling the N cycle in a sediment suspension was investigated by integrating experiments with a biogeochemical model that considers abiotic and biotic processes including chemical adsorption on minerals, aqueous complexation, gas dissolution, microbial metabolism, and necromass dynamics. Biomass was described explicitly in the model with five microbial functional groups and eight different microbial metabolic pathways of inorganic N were accounted for in an ecological feedback loop involving competition and facilitation interrelationships. The model was calibrated and validated against six experiments and captured relatively well the dynamics of N, with 95% of validation tests passing the goodness-of-fit benchmark. In steady state analyses, phototrophic microorganisms appeared to survive competition and dominated the ecosystem in all nutrient leaching scenarios. The competitive and facilitative interactions between microbial functional groups were susceptible to nutrient leaching and the concentrations of dissolved oxygen. For example, heterotrophic microorganisms were outcompeted by phototrophs at high nutrient leaching rates and low O_2(aq) concentration, while both phototrophs and heterotrophs coexisted in facilitative relationship in low nutrient and oxic conditions with heterotrophs providing NH_4^+ to phototrophs through the necromass depolymerization process. Our simulation results show that necromass depolymerization played a very major role in governing the dynamics of sedimentary microbial community and the N cycle.

Notation

Anammox	Anaerobic ammonia oxidation.
B_{DEN}	Denitrifying bacteria.
B_{DNR}	Dissimilatory nitrate reducing bacteria.
B_{HET}	Heterotrophic bacteria.
B_{NIT}	Nitrifying bacteria.
B_{PHOTO}	Phototrophic bacteria.
B_{TOT}	Total living bacteria.
DNR	Dissimilatory nitrate reduction.
IA	Index of agreement.
NABA	Nutrient and biomass affected.
NABF	Nutrient affected and biomass free.
NEC	Necromass.
NFBF	Nutrient and biomass free.
NRMSE	Normalized root-mean-square error.
NOB	Nitrite-oxidizing bacteria.
NSE	Nash-Sutcliffe efficiency.
PBIAS	Percent bias.
R	Correlation coefficient.
SPM	Suspended particulate matter.

Acknowledgments

This project was supported by the Civil Engineering Research and Development Scheme (CERDS) 2015 and the Sydney Research Excellence Initiative (SREI 2020) of The University of Sydney. F. M. was also supported by the Mid Career Research Award (2018) of theUniversity of Sydney and by the Sydney Research Accelerator (SOAR) Fellowship, the University of Sydney. The derivation of microbial metabolic reactions, the experimental raw data, the BRTSim-v2.2g solver, and example of model input and out files can be found in the supporting information. The full package of BRTSim solver can be downloaded at link: https://www.dropbox.com/sh/wrfspx9f1dvuspr/AAD5iA9PsteX3ygAJxQDxAy9a?dl=0. The authors thank the two anonymous reviewers for their comments to the original manuscript.

References

Allen, J., & Clarke, K. (2007). Effects of demersal trawling on ecosystem functioning in the north sea: A modelling study. *Marine Ecology Progress Series*, *336*, 63–75.

Almeida, C., Debacher, N., Downs, A., Cottet, L., & Mello, C. (2009). Removal of methylene blue from colored effluents by adsorption on montmorillonite clay. *Journal of Colloid and Interface Science*, *332*(1), 46–53.

Atkins, P., & De Paula, J. (2005). *Elements of physical chemistry* (4th ed.). USA: Oxford University Press.

Batchelor, B., & Lawrence, A. W. (1978). Autotrophic denitrification using elemental sulfur. *Journal (Water Pollution Control Federation)*, *50*(8), 1986–2001.

Billen, G., Servais, P., & Becquevort, S. (1990). Dynamics of bacterioplankton in oligotrophic and eutrophic aquatic environments: Bottom-up or top-down control? *Hydrobiologia*, *207*(1), 37–42.
Bilotta, G., & Brazier, R. (2008). Understanding the influence of suspended solids on water quality and aquatic biota. *Water Research*, *42*(12), 2849–2861.
Boon, B., & Laudelout, H. (1962). Kinetics of nitrite oxidation by Bitrobacter winogradskyi. *Biochemical Journal*, *85*(3), 440–447.
Brönmark, C., & Hansson, L.-A. (2005). *The biology of lakes and ponds*. New York: Oxford University Press.
Bruce, L. C., Hamilton, D., Imberger, J., Gal, G., Gophen, M., Zohary, T., et al. (2006). A numerical simulation of the role of zooplankton in C, N and P cycling in Lake Kinneret, Israel. *Ecological Modelling*, *193*(3), 412–436.
Callender, E., & Hammond, D. E. (1982). Nutrient exchange across the sediment-water interface in the Potomac River estuary. *Estuarine, Coastal and Shelf Science*, *15*(4), 395–413.
Canfield, D. E., Kristensen, E., & Thamdrup, B. (2005). *Aquatic geomicrobiology*. New York: Academic Press.
Caperon, J., & Meyer, J. (1972). Nitrogen-limited growth of marine phytoplankton—II. Uptake kinetics and their role in nutrient limited growth of phytoplankton. *Deep Sea Research and Oceanographic Abstracts*, *19*, 619–632.
Caron, D. A. (1987). Grazing of attached bacteria by heterotrophic microflagellates. *Microbial Ecology*, *13*(3), 203–218.
Caron, D. A., Davis, P. G., Madin, L. P., & Sieburth, J. M. (1986). Enrichment of microbial populations in macroaggregates (marine snow) from surface waters of the North Atlantic. *Journal of Marine Research*, *44*(3), 543–565.
Cengeloglu, Y., Tor, A., Ersoz, M., & Arslan, G. (2006). Removal of nitrate from aqueous solution by using red mud. *Separation and Purification Technology*, *51*(3), 374–378.
Cochlan, W. P., & Harrison, P. J. (1991). Kinetics of nitrogen (nitrate, ammonium and urea) uptake by the picoflagellate Micromonas pusilla (prasinophyceae). *Journal of Experimental Marine Biology and Ecology*, *153*(2), 129–141.
Cole, J. J. (1982). Interactions between bacteria and algae in aquatic ecosystems. *Annual Review of Ecology and Systematics*, *13*, 291–314.
Copcia, V., Hristodor, C., Luchian, C., Bilba, N., & Sandu, I. (2010). Ammonium nitrogen removal from aqueous solution by natural clay. *Revista de Chimie (Bucharest)*, *61*, 1192–1196.
Dalsgaard, T., Thamdrup, B., & Canfield, D. E. (2005). Anaerobic ammonium oxidation (anammox) in the marine environment. *Research in Microbiology*, *156*(4), 457–464.
Dang, H., & Chen, C.-T. A. (2017). Ecological energetic perspectives on responses of nitrogen-transforming chemolithoautotrophic microbiota to changes in the marine environment. *Frontiers in Microbiology*, *8*, 1246.
Dang, H., & Lovell, C. R. (2016). Microbial surface colonization and biofilm development in marine environments. *Microbiology and Molecular Biology Reviews*, *80*(1), 91–138.
Davies, K. J., Lloyd, D., & Boddy, L. (1989). The effect of oxygen on denitrification in Paracoccus denitrificans and pseudomonas aeruginosa. *Microbiology*, *135*(9), 2445–2451.
De Brouwer, J., Bjelic, S., De Deckere, E., & Stal, L. (2000). Interplay between biology and sedimentology in a mudflat (Biezelingse Ham, Westerschelde, The Netherlands). *Continental Shelf Research*, *20*(10), 1159–1177.
Doherty, J. (2005). *PEST: Model-independent parameter estimation* (5th ed.). Australia: Watermark Computing, Corinda.
Duarte, C. M., & Cebrian, J. (1996). The fate of marine autotrophic production. *Limnology and Oceanography*, *41*(8), 1758–1766.
Dworkin, M., Falkow, S., Rosenberg, E., Schleifer, K.-H., & Stackebrandt, E. (2006). *The prokaryotes: Vol. 2: Ecophysiology and biochemistry*. New York: Springer Science & Business Media.
Ebeling, J. M., Timmons, M. B., & Bisogni, J. (2006). Engineering analysis of the stoichiometry of photoautotrophic, autotrophic, and heterotrophic removal of ammonia–nitrogen in aquaculture systems. *Aquaculture*, *257*(1), 346–358.
Ebrahimi, A., & Or, D. (2015). Hydration and diffusion processes shape microbial community organization and function in model soil aggregates. *Water Resources Research*, *51*, 9804–9827. https://doi.org/10.1002/2015WR017565
Eppley, R. W., & Coatsworth, J. L. (1968). Uptake of nitrate and nitrite by ditylum brightwellii-kinetics and mechanisms12. *Journal of Phycology*, *4*(2), 151–156.
Goldman, J., & Dennett, M. (1991). Ammonium regeneration and carbon utilization by marine bacteria grown on mixed substrates. *Marine Biology*, *109*(3), 369–378.
Golterman, H. L., Sly, P. G., & Thomas, R. L. (1983). *Study of the relationship between water quality and sediment transport: A guide for the collection and interpretation of sediment quality data*. New York: UNIPUB.
Gottschalk, G. (1986). *Bacterial metabolism*. New York: Springer Science & Business Media.
Goulder, R. (1977). Attached and free bacteria in an estuary with abundant suspended solids. *Journal of applied Bacteriology*, *43*(3), 399–405.
Green, M. O., & Coco, G. (2014). Review of wave-driven sediment resuspension and transport in estuaries. *Reviews of Geophysics*, *52*, 77–117. https://doi.org/10.1002/2013RG000437
Groffman, P. M., & Bohlen, P. J. (1999). Soil and sediment biodiversity: Cross-system comparisons and large-scale effects. *BioScience*, *49*(2), 139–148.
Grossart, H., Kiørboe, T., Tang, K., Allgaier, M., Yam, E., & Ploug, H. (2006). Interactions between marine snow and heterotrophic bacteria: Aggregate formation and microbial dynamics. *Aquatic Microbial Ecology*, *42*, 19–26.
Grossart, H.-P., Tang, K. W., Kiørboe, T., & Ploug, H. (2007). Comparison of cell-specific activity between free-living and attached bacteria using isolates and natural assemblages. *FEMS Microbiology Letters*, *266*(2), 194–200.
Gu, C., Anderson, W., & Maggi, F. (2012). Riparian biogeochemical hot moments induced by stream fluctuations. *Water Resources Research*, *48*, W09546. https://doi.org/10.1029/2011WR011720
Guerrero, R., Pedrós-Alió, C., Esteve, I., Mas, J., Chase, D., & Margulis, L. (1986). Predatory prokaryotes: Predation and primary consumption evolved in bacteria. *Proceedings of the National Academy of Sciences*, *83*(7), 2138–2142.
Horner-Devine, M. C., Carney, K. M., & Bohannan, B. J. (2004). An ecological perspective on bacterial biodiversity. *Proceedings of the Royal Society of London B: Biological Sciences*, *271*(1535), 113–122.
Howarth, R. W., Marino, R., Lane, J., & Cole, J. J. (1988). Nitrogen fixation in freshwater, estuarine, and marine ecosystems. 1. Rates and importance. *Limnology and Oceanography*, *33*(4part2), 669–687.
Jones, C. G., Lawton, J. H., & Shachak, M. (1994). Organisms as ecosystem engineers, *Ecosystem Management* (pp. 130–147). New York: Springer.
Kalvelage, T., Jensen, M. M., Contreras, S., Revsbech, N. P., Lam, P., Günter, M., et al. (2011). Oxygen sensitivity of anammox and coupled N-cycle processes in oxygen minimum zones. *PloS One*, *6*(12), e29299.
Kaufman, A. G., & Borrett, S. R. (2010). Ecosystem network analysis indicators are generally robust to parameter uncertainty in a phosphorus model of Lake Sidney Lanier, USA. *Ecological Modelling*, *221*(8), 1230–1238.

Kelly, D. P. (1971). Autotrophy: Concepts of lithotrophic bacteria and their organic metabolism. *Annual Reviews in Microbiology*, *25*(1), 177–210.
Kiørboe, T., Grossart, H.-P., Ploug, H., & Tang, K. (2002). Mechanisms and rates of bacterial colonization of sinking aggregates. *Applied and Environmental Microbiology*, *68*(8), 3996–4006.
Kiørboe, T., Tang, K., Grossart, H.-P., & Ploug, H. (2003). Dynamics of microbial communities on marine snow aggregates: Colonization, growth, detachment, and grazing mortality of attached bacteria. *Applied and Environmental Microbiology*, *69*(6), 3036–3047.
Kiørboe, T., Grossart, H.-P., Ploug, H., Tang, K., & Auer, B. (2004). Particle-associated flagellates: Swimming patterns, colonization rates, and grazing on attached bacteria. *Aquatic Microbial Ecology*, *35*(2), 141–152.
Kirchman, D. L. (2002). The ecology of cytophaga–flavobacteria in aquatic environments. *FEMS Microbiology Ecology*, *39*(2), 91–100.
Kirchman, D. L., & Wheeler, P. A. (1998). Uptake of ammonium and nitrate by heterotrophic bacteria and phytoplankton in the sub-Arctic Pacific. *Deep Sea Research Part I: Oceanographic Research Papers*, *45*(2), 347–365.
Kits, K. D., Sedlacek, C. J., Lebedeva, E. V., Han, P., Bulaev, A., Pjevac, P., et al. (2017). Kinetic analysis of a complete nitrifier reveals an oligotrophic lifestyle. *Nature*, *549*(7671), 269–272.
Knicker, H., & Hatcher, P. G. (1997). Survival of protein in an organic-rich sediment: Possible protection by encapsulation in organic matter. *Die Naturwissenschaften*, *84*(6), 231–234.
Kranck, K. (1973). Flocculation of suspended sediment in the sea. *Nature*, *246*, 348–350.
Langmuir, I. (1918). The adsorption of gases on plane surfaces of glass, mica and platinum.*Journal of the American Chemical society*, *40*(9), 1361–1403.
Levenberg, K. (1944). A method for the solution of certain non-linear problems in least squares. *Quarterly of Applied Mathematics*, *2*(2), 164–168.
Li, Z., & Bowman, R. S. (2001). Retention of inorganic oxyanions by organo-kaolinite. *Water Research*, *35*(16), 3771–3776.
Lubarsky, H. V., Hubas, C., Chocholek, M., Larson, F., Manz, W., Paterson, D. M., et al. (2010). The stabilisation potential of individual and mixed assemblages of natural bacteria and microalgae. *PloS one*, *5*(11), e13794.
MacIsaac, J., & Dugdale, R. (1969). The kinetics of nitrate and ammonia uptake by natural populations of marine phytoplankton. *Deep Sea Research and Oceanographic Abstracts*, *16*, 45–57.
Madigan, M. T., Clark, D. P., Stahl, D., & Martinko, J. M. (2010). *Brock biology of microorganisms 13th edition*: Benjamin Cummings.
Maggi, F. (2005). Flocculation dynamics of cohesive sediment (PhD thesis). Delft University of Technology, TU Delft.
Maggi, F. (2009). Biological flocculation of suspended particles in nutrient-rich aqueous ecosystems. *Journal of Hydrology*, *376*(1), 116–125.
Maggi, F. (2015a). Brtsim version 1: A general-purpose multiphase and multicomponent computational solver for biogeochemical reaction-advection-dispersion processes in porous and non-porous media (Tech. Rep. Research Report R954, 1st edn.). Australia: The University of Sydney.
Maggi, F. (2015b). Experimental evidence of how the fractal structure controls the hydrodynamic resistance on granular aggregates moving through water. *Journal of Hydrology*, *528*, 694–702.
Maggi, F., & Riley, W. J. (2017). Near activation and differential activation in enzymatic reactions. *International Journal of Chemical Kinetics*, *49*(5), 305–318.
Maggi, F., & Tang, F. H. (2015). Analysis of the effect of organic matter content on the architecture and sinking of sediment aggregates. *Marine Geology*, *363*, 102–111.
Matson, E. A., & Brinson, M. M. (1990). Stable carbon isotopes and the C: N ratio in the estuaries of the Pamlico and Neuse Rivers, North Carolina. *Limnology and Oceanography*, *35*(6), 1290–1300.
McCarthy, J. J., Taylor, W. R., & Taft, J. L. (1977). Nitrogenous nutrition of the plankton in the Chesapeake Bay. 1. Nutrient availability and phytoplankton preferences. *Limnology and Oceanography*, *22*(6), 996–1011.
McCave, I. (1984). Size spectra and aggregation of suspended particles in the deep ocean. *Deep Sea Research Part A: Oceanographic Research Papers*, *31*(4), 329–352.
McCready, S., Birch, G. F., & Long, E. R. (2006). Metallic and organic contaminants in sediments of Sydney Harbour, Australia and vicinity—A chemical dataset for evaluating sediment quality guidelines. *Environment International*, *32*(4), 455–465.
Meadows, P. S., Meadows, A., & Murray, J. M. (2012). Biological modifiers of marine benthic seascapes: Their role as ecosystem engineers. *Geomorphology*, *157*, 31–48.
Monod, J. (1949). The growth of bacterial cultures. *Annual Reviews in Microbiology*, *3*(1), 371–394.
Montserrat, F., Van Colen, C., Degraer, S., Ysebaert, T., & Herman, P. M. (2008). Benthic community-mediated sediment dynamics. *Marine Ecology Progress Series*, *372*, 43–59.
Nash, J. E., & Sutcliffe, J. V. (1970). River flow forecasting through conceptual models part I—A discussion of principles. *Journal of hydrology*, *10*(3), 282–290.
Newell, S. E., Pritchard, K. R., Foster, S. Q., & Fulweiler, R. W. (2016). Molecular evidence for sediment nitrogen fixation in a temperate New England estuary. *PeerJ*, *4*, e1615.
Pernthaler, J. (2005). Predation on prokaryotes in the water column and its ecological implications. *Nature Reviews Microbiology*, *3*(7), 537–546.
Pind, A., Risgaard-Petersen, N., & Revsbech, N. P. (1997). Denitrification and microphytobenthic NO_3^- consumption in a Danish low land stream: Diurnal and seasonal variation. *Aquatic Microbial Ecology*, *12*(3), 275–284.
Prokopkin, I., Mooij, W., Janse, J., & Degermendzhy, A. (2010). A general one-dimensional vertical ecosystem model of Lake Shira (Russia, Khakasia): Description, parametrization and analysis. *Aquatic Ecology*, *44*(3), 585–618.
Raven, J. A. (2009). Contributions of anoxygenic and oxygenic phototrophy and chemolithotrophy to carbon and oxygen fluxes in aquatic environments. *Aquatic Microbial Ecology*, *56*, 177–192. Inter-Research.
Reay, D. S., Nedwell, D. B., Priddle, J., & Ellis-Evans, J. C. (1999). Temperature dependence of inorganic nitrogen uptake: Reduced affinity for nitrate at suboptimal temperatures in both algae and bacteria. *Applied and Environmental Microbiology*, *65*(6), 2577–2584.
Riley, W., Maggi, F., Kleber, M., Torn, M., Tang, J., Dwivedi, D., et al. (2014). Long residence times of rapidly decomposable soil organic matter: Application of a multi-phase, multi-component, and vertically resolved model (BAMS1) to soil carbon dynamics. *Geoscientific Model Development*, *7*, 1335–1355.
Rittmann, B. E., & McCarty, P. L. (2001). *Environmental biotechnology: Principles and applications*. New York: McGrawHill.
Rizzo, W. M. (1990). Nutrient exchanges between the water column and a subtidal benthic microalgal community. *Estuaries*, *13*(3), 219–226.
Robson, B. J. (2014). State of the art in modelling of phosphorus in aquatic systems: Review, criticisms and commentary. *Environmental Modelling & Software*, *61*, 339–359.
Saleh-Lakha, S., Shannon, K. E., Henderson, S. L., Goyer, C., Trevors, J. T., Zebarth, B. J., et al. (2009). Effect of ph and temperature on denitrification gene expression and activity in Pseudomonas mandelii. *Applied and Environmental Microbiology*, *75*(12), 3903–3911.

Servais, P., Billen, G., & Rego, J. V. (1985). Rate of bacterial mortality in aquatic environments. *Applied and Environmental Microbiology*, *49*(6), 1448–1454.
Siviglia, A., & Crosato, A. (2016). Numerical modelling of river morphodynamics: Latest developments and remaining challenges. *Advances in Water Resources*, *93*, 1–3.
Sorooshian, S., Duan, Q., & Gupta, V. K. (1993). Calibration of rainfall-runoff models: Application of global optimization to the Sacramento soil moisture accounting model. *Water Resources Research*, *29*(4), 1185–1194.
Tang, F. H. M., & Maggi, F. (2015). A laboratory facility for flocculation-related experiments (Tech. Rep. Research Report R952). Australia: The University of Sydney.
Tang, F. H. M., & Maggi, F. (2016). A mesocosm experiment of suspended particulate matter dynamics in nutrient-and biomass-affected waters. *Water Research*, *89*, 76–86.
Toffolon, M. (2002). Hydrodynamics and morphodynamics of tidal channels (PhD thesis). PhD thesis University of Padova, Italy.
Toseland, A., Daines, S. J., Clark, J. R., Kirkham, A., Strauss, J., Uhlig, C., et al. (2013). The impact of temperature on marine phytoplankton resource allocation and metabolism. *Nature Climate Change*, *3*(11), 979–984.
Tourna, M., Freitag, T. E., Nicol, G. W., & Prosser, J. I. (2008). Growth, activity and temperature responses of ammonia-oxidizing archaea and bacteria in soil microcosms. *Environmental Microbiology*, *10*(5), 1357–1364.
Tufail, A. (1987). Microbial communities colonising nutrient-enriched marine sediment. *Hydrobiologia*, *148*(3), 245–255.
Turley, C., & Mackie, P. (1994). Biogeochemical significance of attached and free-living bacteria and the flux of particles in the NE Atlantic Ocean. *Marine Ecology-Progress Series*, *115*, 191–191.
Van Kessel, J. (1977). Factors affecting the denitrification rate in two water-sediment systems. *Water Research*, *11*(3), 259–267.
Wall, D. H., Palmer, M. A., & Snelgrove, P. V. (2001). Biodiversity in critical transition zones between terrestrial, freshwater, and marine soils and sediments: Processes, linkages, and management implications. *Ecosystems*, *4*(5), 418–420.
Wang, Y., Chen, H., Liu, Y.-X., Ren, R.-P., & Lv, Y.-K. (2015). Effect of temperature, salinity, heavy metals, ammonium concentration, ph and dissolved oxygen on ammonium removal by an aerobic nitrifier. *RSC Advances*, *5*(97), 79,988–79,996.
Willmott, C. J. (1982). Some comments on the evaluation of model performance. *Bulletin of the American Meteorological Society*, *63*(11), 1309–1313.
Willmott, C. J., Ackleson, S. G., Davis, R. E., Feddema, J. J., Klink, K. M., Legates, D. R., et al. (1985). Statistics for the evaluation and comparison of models. *Journal of Geophysical Research*, *90*(C5), 8995–9005.
Wilson, G. S., Raftos, D. A., Corrigan, S. L., & Nair, S. V. (2010). Diversity and antimicrobial activities of surface-attached marine bacteria from Sydney Harbour, Australia. *Microbiological Research*, *165*(4), 300–311.
Wilson, J. (2006). The role of benthic microalgae in the ecology of Lake Illawarra. *Wetlands (Australia)*, *21*(2), 94.
Wolery, T. J. (1992). EQ3/6: A software package for geochemical modeling of aqueous systems: Package overview and installation guide (version 7.0), Lawrence Livermore National Laboratory Livermore, CA.